TECHNICAL REPORTS

nature neuroscience

A transcriptional reporter of intracellular Ca^{2+} in *Drosophila*

Xiaojing J Gao[1], Olena Riabinina[2], Jiefu Li[1], Christopher J Potter[2], Thomas R Clandinin[3] & Liqun Luo[1,3]

Intracellular Ca^{2+} is a widely used neuronal activity indicator. Here we describe a transcriptional reporter of intracellular Ca^{2+} (TRIC) in *Drosophila* that uses a binary expression system to report Ca^{2+}-dependent interactions between calmodulin and its target peptide. We found that *in vitro* assays predicted *in vivo* properties of TRIC and that TRIC signals in sensory systems depend on neuronal activity. TRIC was able to quantitatively monitor neuronal responses that changed slowly, such as those of neuropeptide F–expressing neurons to sexual deprivation and neuroendocrine pars intercerebralis cells to food and arousal. Furthermore, TRIC-induced expression of a neuronal silencer in nutrient-activated cells enhanced stress resistance, providing a proof of principle that TRIC can be used for circuit manipulation. Thus, TRIC facilitates the monitoring and manipulation of neuronal activity, especially those reflecting slow changes in physiological states that are poorly captured by existing methods. TRIC's modular design should enable optimization and adaptation to other organisms.

© 2015 Nature America, Inc. All rights reserved.

Live imaging of Ca^{2+} with fluorescent indicators is a powerful technique for monitoring neural circuit dynamics[1,2]. Here we describe TRIC, which captures changes in neuronal activity over long timescales, complementing several limitations of fluorescent indicators. First, functional imaging is usually performed acutely and invasively in restrained animals. As a result, it is difficult to monitor circuits whose activities vary slowly with changes in the physiological state[3,4]. These circuits often use modulatory neurotransmitters or neuropeptides, and their outputs can cause the same neural network to mediate starkly different behaviors[5]. How the activity of modulatory neurons is regulated under natural conditions remains poorly understood given the absence of suitable tools. Second, because functional imaging and electrophysiology are time consuming, they have limited capacity to interrogate complex circuits systematically. For instance, serial electron microscopic reconstruction has revealed dozens of prominent connections in one of the flies' visual centers, the medulla[6]. Systematic interrogation of these connections would involve hundreds or thousands of experiments that inactivate specific input neurons, monitor output neurons and present specific stimuli, which are extremely challenging with existing methods. Third, functional imaging is limited by the field of view accessible to a microscope. Thus, behaviorally relevant changes in neuronal activity in widely distributed brain regions can be difficult to monitor in parallel. Finally, Ca^{2+} imaging allows visualization of neuronal activity, but does not enable subsequent genetic manipulation of active cells.

An alternative approach to monitoring neural activity is based on the activation of immediate early genes (IEGs), whose expression is increased when neurons are active. Such endogenous transcriptional reporters of activity have been widely used in vertebrate models and have provided a complementary approach to live imaging of calcium signals[7]. In addition, other effectors have been placed under the control of IEG enhancers and promoters for genetic manipulation of active neurons[8–11]. However, only one IEG has recently been described in fruit flies[12], and alternative methods for monitoring neuronal activity using transcriptional reporters are scarce[13]. Moreover, the mechanism of IEG induction by neuronal activity is still not well understood, hindering the optimization and general application of this strategy.

To address the limitations of calcium-imaging experiments, we developed TRIC to integrate changes in Ca^{2+} levels over long periods of time in freely behaving animals. TRIC takes advantage of Ca^{2+}-dependent interactions between calmodulin and its target peptides[14] and reports this interaction using a binary expression system (**Fig. 1a**). TRIC produces a stable signal that can be monitored in fixed tissue, increasing the throughput of experiments that interrogate functional connectivity and allowing for visualization of neuronal activity in the whole brain. In addition, TRIC allows for subsequent expression of any transgenes, so that one can selectively manipulate active neurons. We tested TRIC in flies, given the well-established use of split binary systems[15,16] and the potential of combining TRIC with other genetic tools. We provide proof-of-principle experiments using TRIC in cultured cells and in visual, olfactory and neuromodulatory systems *in vivo*. When applied to pars intercerebralis (PI) cells[17], TRIC validated previously known regulatory factors, revealed distinct modes of PI response to different physiological conditions and enhanced stress resistance through the activity-dependent expression of a synaptic transmission blocker.

RESULTS

Selecting TRIC components in cultured cells and flies

To build a transcriptional reporter of intracellular Ca^{2+} levels, we fused calmodulin (CaM) and its target peptide[14] to a transcriptional activation domain (AD) and a DNA-binding domain (DBD), respectively. When CaM binds to its target peptide in the presence of Ca^{2+},

[1]Howard Hughes Medical Institute and Department of Biology, Stanford University, Stanford, California, USA. [2]The Solomon H. Snyder Department of Neuroscience, The Johns Hopkins University School of Medicine, Baltimore, Maryland, USA. [3]Department of Neurobiology, Stanford University, Stanford, California, USA. Correspondence should be addressed to X.J.G. (xjgao@alumni.stanford.edu), T.R.C. (trc@stanford.edu) or L.L. (lluo@stanford.edu).

Received 3 February; accepted 13 April; published online 11 May 2015; doi:10.1038/nn.4016

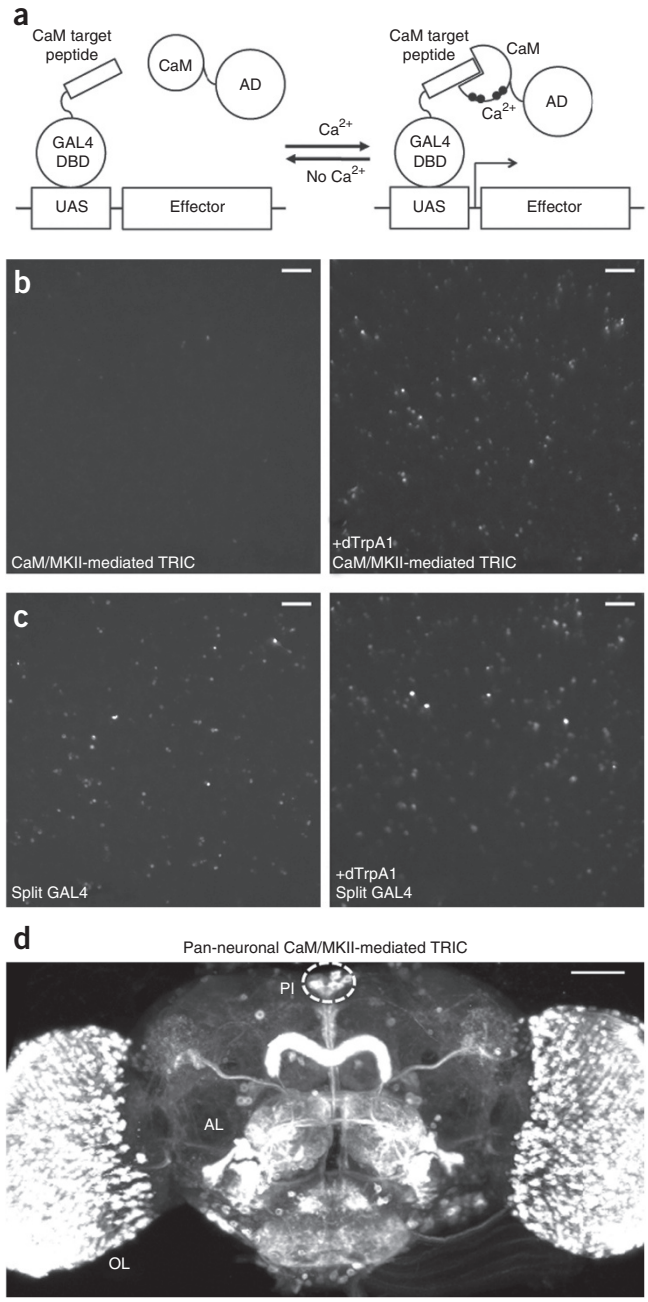

Figure 1 Proof of principle of TRIC in cultured cells and transgenic flies. (**a**) The design of TRIC. Ca^{2+} mediates the binding of CaM and its targeting peptide, thereby bringing a transcriptional AD (fused with CaM) to the DBD of a transcription factor (here yeast GAL4, fused with CaM-target peptide) and activating transcription of an effector that is under the control of UAS. The binding of two fusion proteins depends on Ca^{2+} concentration. (**b**) CaM/MKII-mediated TRIC (*ActP-MKII::GAL4DBDo*, *ActP-p65AD::CaM*). The *UAS-GFP* expression (right) was much weaker and sparser in the absence of *ActP-dTrpA1* (left). (**c**) Split GAL4s that bind constitutively via leucine zippers (Zp) were used as a positive control (*ActP-Zp::GAL4DBD*, *ActP-VP16AD::Zp*). The *UAS-GFP* expression was independent of *ActP-dTrpA1*. Cells in **b** and **c** were all subjected to the same repetitive heat shocks. (**d**) CaM/MKII-mediated TRIC signal in the brain of transgenic flies (*nsyb-MKII::GAL4DBDo*, *QUAS-p65AD::CaM*, *nsyb-QF2*, *tubP-QS*, *UAS-mCD8::RFP*, representative of ten samples). OL, optic lobe; AL, antennal lobe. In this and subsequent figures, unless specified, the maximal projections of confocal image stacks are shown and the scale bars represent 50 μm.

the reconstituted transcription factor was able to express an effector (**Fig. 1a**). We performed initial tests of TRIC efficiency in *Drosophila* S2 cells. We induced pulses of Ca^{2+} influx by heat-shocking cells transfected with a temperature-gated cation channel, dTrpA1 (ref. 18). We tested two DBDs, two ADs[16] and three CaM-target peptides[19] (**Fig. 1b**, **Supplementary Table 1** and **Supplementary Fig. 1a**,**b**). We found that the TRIC version with the best signal-to-noise ratio in cultured cells consists of the codon-optimized GAL4 DBD (GAL4DBDo) fused with the CaM-target peptide in CaMKII (MKII) and the p65 AD fused with CaM.

In the absence of dTrpA1, CaM/MKII-mediated TRIC expressed little of the co-transfected *UAS-GFP* reporter (**Fig. 1b**). In contrast, heat-induced Ca^{2+} influx through dTrpA1 resulted in robust GFP expression (**Fig. 1b**). The CaM/MKII-mediated TRIC signal was comparable to that of constitutively dimerizing split GAL4 (ref. 15) (**Fig. 1b**,**c**), which was independent of dTrpA1 (**Fig. 1c**).

To test TRIC *in vivo*, we generated transgenic flies in which *MKII::GAL4DBDo* was expressed using a pan-neuronal promoter (*nsyb*) and *p65AD::CaM* was controlled by *QUAS* from the Q system[20]. The *p65AD::CaM* was expressed by the *nsyb*-driven transcription factor QF2 (ref. 21) and suppressed by the ubiquitously expressed suppressor QS. Adding quinic acid (QA) relieves QS suppression[20], allowing us to tune the expression level of TRIC. In the test flies exposed to QA, we observed strong TRIC signal throughout the brain (**Fig. 1d**) and the ventral nerve cord (**Supplementary Fig. 1d**). Consistent with the difference *in vitro* (**Fig. 1b** and **Supplementary Fig. 1a**), M13, the CaM-target peptide in smooth muscle myosin light chain kinase, produced weaker signals than MKII *in vivo* (**Fig. 1d** and **Supplementary Fig. 1c**). Thus, for subsequent experiments, we chose *MKII::GAL4DBDo* and *p65AD::CaM* as the core TRIC components.

TRIC signals in the optic lobes depend on visual input

To characterize TRIC's ability to detect changes in neural activity, we started with the optic lobes, which process visual information. In pan-neuronal TRIC flies raised in ambient light, robust signal was detected across the optic lobes (**Fig. 2a**). In contrast, the signal was nearly abolished (**Fig. 2a**) when we introduced a *norpA* mutation, that eliminates phototransduction[22].

To test whether sensory experience can modulate the TRIC signal, we raised flies in darkness until eclosion, induced *p65AD::CaM* expression with QA, and then kept animals in ambient light or darkness for 3 d. However, the ambient light did not significantlyelevate TRIC signal ($P = 0.14$; **Supplementary Fig. 2a**). We hypothesized that, unlike *norpA* mutants, dark-reared flies would still have spontaneous photoreceptor activity that could propagate to optic lobe neurons and be detected by TRIC. Such a low level of activity might saturate TRIC signal in darkness with an exceptionally stable mCD8::fluorescent protein (mCD8::FP) reporter. Indeed, we found significant reduction ($P < 0.0001$) of TRIC signal in dark rearing compared with light exposure when we used a less stable *nsyb::GFP* reporter[23] (**Supplementary Fig. 2b**,**c**) or when we restricted reporter availability temporally using a *UAS-FRT-stop-FRT-mCD8::GFP* reporter[24] that is dependent on heat-shock induction of a FLP recombinase (**Supplementary Fig. 2d**). Thus, with appropriate reporters, TRIC can discriminate between the complete absence of phototransduction, spontaneous activity in darkness and the response to light.

Next, we used FLP-mediated recombination to regulate expression of the TRIC component *QUAS-FRT-stop-FRT-p65AD::CaM* directly. As we observed before, light exposure induced strong and dense TRIC labeling in the optic lobes after heat shock–induced onset of *p65AD::CaM*

© 2015 Nature America, Inc. All rights reserved.

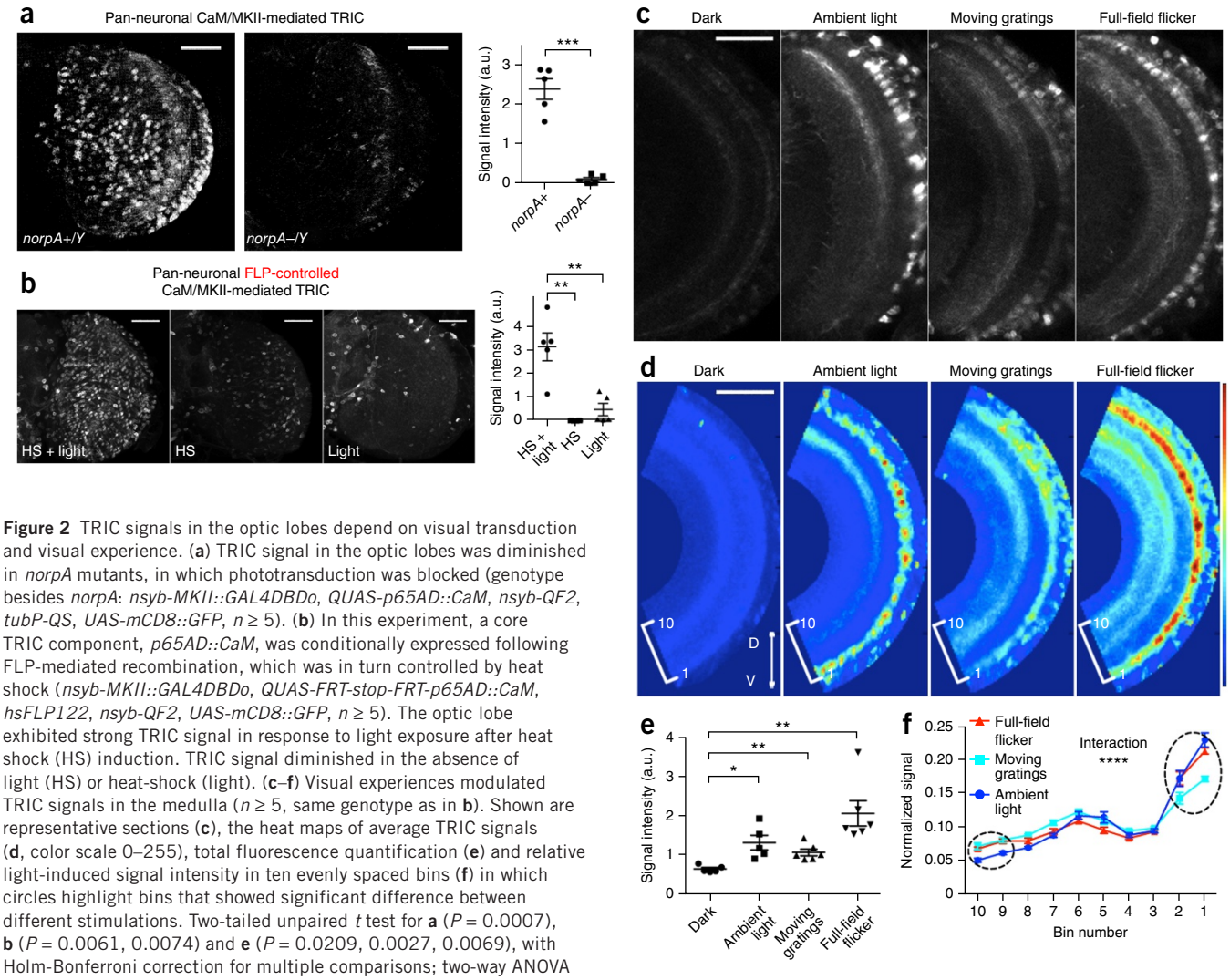

Figure 2 TRIC signals in the optic lobes depend on visual transduction and visual experience. (**a**) TRIC signal in the optic lobes was diminished in *norpA* mutants, in which phototransduction was blocked (genotype besides *norpA*: *nsyb-MKII::GAL4DBDo*, *QUAS-p65AD::CaM*, *nsyb-QF2*, *tubP-QS*, *UAS-mCD8::GFP*, $n \geq 5$). (**b**) In this experiment, a core TRIC component, *p65AD::CaM*, was conditionally expressed following FLP-mediated recombination, which was in turn controlled by heat shock (*nsyb-MKII::GAL4DBDo*, *QUAS-FRT-stop-FRT-p65AD::CaM*, *hsFLP122*, *nsyb-QF2*, *UAS-mCD8::GFP*, $n \geq 5$). The optic lobe exhibited strong TRIC signal in response to light exposure after heat shock (HS) induction. TRIC signal diminished in the absence of light (HS) or heat-shock (light). (**c**–**f**) Visual experiences modulated TRIC signals in the medulla ($n \geq 5$, same genotype as in **b**). Shown are representative sections (**c**), the heat maps of average TRIC signals (**d**, color scale 0–255), total fluorescence quantification (**e**) and relative light-induced signal intensity in ten evenly spaced bins (**f**) in which circles highlight bins that showed significant difference between different stimulations. Two-tailed unpaired *t* test for **a** ($P = 0.0007$), **b** ($P = 0.0061$, 0.0074) and **e** ($P = 0.0209$, 0.0027, 0.0069), with Holm-Bonferroni correction for multiple comparisons; two-way ANOVA for **f** (interaction $P < 0.0001$), with Tukey *post hoc* comparisons. Scale bars in all panels represent 50 µm. $^{*}P < 0.05$, $^{**}P < 0.01$, $^{***}P < 0.001$, $^{****}P < 0.0001$. The data are presented as mean ± s.e.m.; scatter plots show data points. Key changes of genetic components are colored red.

© 2015 Nature America, Inc. All rights reserved.

expression (**Fig. 2b**). Omitting either light or heat shock markedly reduced TRIC signals (**Fig. 2b**).

We also used FLP-regulated TRIC onset to test whether different visual stimuli trigger distinct TRIC patterns in the medulla, the second optic ganglion. We heat-shocked FLP-regulated TRIC flies and then exposed them to darkness, ambient light, moving gratings or full-field flicker; the latter two stimuli are commonly used in visual system studies[25]. These stimuli increased the overall fluorescent intensity in medulla to different extents (**Fig. 2c**–**e**) and different stimuli appeared to preferentially induce TRIC signal in different layers, as was evident in individual samples (**Fig. 2c**) or average heat maps after image registration of multiple flies (**Fig. 2d**,**f** and Online Methods). Thus, with the FLP-regulated temporal control, TRIC can report both the overall activity level of the optic lobes and layer-specific activation in the medulla in response to different visual stimuli.

Characterizing TRIC in the olfactory projection neurons

Many optic lobe neurons use graded potentials. To test whether TRIC can monitor neurons with action potentials, we turned to the spiking olfactory projection neurons (PNs) labeled by *GH146-QF*[20]. For flies raised under standard conditions, TRIC labeled PN cell bodies around, and dendrites in, the antennal lobes (**Fig. 3a**). These signals were markedly reduced by genetic ablation of the olfactory receptor neurons (ORNs), the primary presynaptic partners of PNs (**Fig. 3a**).

To abolish sensory input acutely, we removed the antennae, which contain the majority of ORNs. An *nsyb::GFP* reporter showed significant signal reduction 5 d after bilateral antennectomy ($P < 0.0001$; **Fig. 3b**), and this was not a result of axon degeneration (**Supplementary Fig. 3a**). Given that ORNs project bilaterally and that PNs only innervate the ipsilateral antennal lobe, we tested the consequence of unilateral antennectomy. This manipulation did not reduce PN signal compared with intact flies (**Fig. 3b**), and the signals in the ipsilateral and contralateral antennal lobes were similar (**Fig. 3b** and **Supplementary Fig. 3b**), consistent with the reported small differences between the spiking rates in PNs caused by contra- and ipsilateral inputs[26]. This results suggest that single-antenna input saturates PN responses in both hemispheres, reflecting a ceiling effect in PNs or TRIC. Moreover, a luciferase reporter also detected antennectomy-induced TRIC signal reduction (**Fig. 3c** and **Supplementary Fig. 3c**) and the artificial activation of PNs (**Supplementary Fig. 3d**).

The PNs were characterized for the only reported transcriptional indicator of neuronal activity in flies (CaLexA), a NFAT-LexA chimera

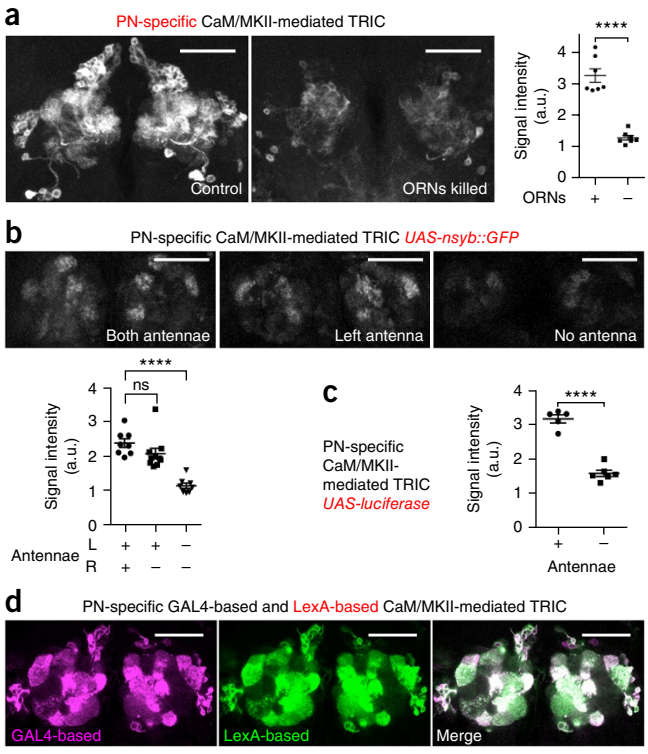

Figure 3 Characterization of TRIC in olfactory PNs. (**a**) Genetic ablation of ORNs reduced TRIC signal in PNs (*nsyb-MKII::GAL4DBDo*, *QUAS-p65AD::CaM*, *GH146-QF*, *UAS-mCD8::GFP*; $n \geq 7$). Right image, expression of ricin toxin A (RTA) was restricted to the ORNs (+*peb-GAL4*, *ey-FLP*, *UAS-FRT-w+-FRT-RTA*), where the *ey* enhancer expressed FLP to remove *w+*, and the *peb-GAL4* drove RTA expression in ORNs. (**b**) Bilateral, but not unilateral, antenna removal reduced TRIC signal, using *nsyb::GFP* as the reporter (*nsyb-MKII::GAL4DBDo*, *QUAS-p65AD::CaM*, *GH146-QF*, *UAS-nsyb::GFP*, $n \geq 8$). (**c**) A luciferase reporter detected the reduction of TRIC signal by antenna removal ($n \geq 5$). (**d**) Similarity in PN labeling between GAL4-based and LexA-based TRICs (*nsyb-MKII::GAL4DBDo*, *nsyb-MKII::nlsLexADBDo*, *QUAS-p65AD::CaM*, *GH146-QF*, *UAS-mCD8::RFP*, *lexAop2-mCD8::GFP*, representative of ten brains). Shown are single confocal slices. Two-tailed unpaired *t* test for **a** ($P < 0.0001$), **b** ($P = 0.1384$, <0.0001) and **c** ($P < 0.0001$), with Holm-Bonferroni correction for multiple comparisons. Scale bars in all panels represent 50 µm. $^{****}P < 0.0001$. ns, not significant. Key changes of genetic components are colored red. Data are presented as mean ± s.e.m.

whose transcriptional activity is based on the Ca^{2+}-regulated dephosphorylation and nuclear translocation of NFAT[13]. We replaced GAL4 DBD with LexA DBD to directly compare the performance of TRIC and CaLexA. We found that LexA-based TRIC labeled PNs broadly and strongly (**Supplementary Fig. 4a**), matching the performance of GAL4-based TRIC in cell bodies and the neuropil (**Fig. 3d**). In contrast, CaLexA only labeled two PN classes (**Supplementary Fig. 4b**). Pan-neuronal CaLexA signal was also much weaker and sparser than TRIC (**Fig. 1d** and **Supplementary Fig. 4c**). These results also suggest that TRIC is robust to substitution of the DBD modules.

Monitoring neuromodulatory circuits with TRIC

TRIC relies on the relatively slow process of reporter expression. It is therefore well suited for monitoring neuromodulatory circuits, whose activities often vary with an animal's physiological states on a time scale too long for traditional reporters. Having characterized TRIC in the sensory systems, we next turned to investigate its utility in modulatory circuits. We first tested whether TRIC signal can generally be detected in various modulatory neurons. To make TRIC compatible with existing GAL4 drivers, we used *nsyb-MKII::nlsLexADBDo* (**Fig. 3d**), together with *p65AD:CaM* driven by UAS. For modulatory neurotransmitters, we tested dopaminergic[27], serotonergic[28], and tyraminergic and octopaminergic[29] neurons (**Supplementary Fig. 5a–c**); we also tested neurons expressing neuropeptide F (NPF)[30] (**Fig. 4a**) and general neuropeptidergic neurons[31] (**Supplementary Fig. 5d**). In all cases, TRIC was able to visualize Ca^{2+} in various proportions of $GAL4^+$ neurons.

We noted that, although TRIC signal was high in many modulatory neurons, it was undetectable in others (**Fig. 4a** and **Supplementary Fig. 5a–d**). Indeed, in our initial pan-neuronal TRIC, signals were sparser than would be expected if every $nsyb^+$ neuron was able to convert activity into a TRIC signal (**Fig. 1d**). Such heterogeneity could reflect different levels of neuronal activity, but could also reflect differences in the ratio between DBD and AD expression. Specifically, in a scenario in which DBD components outnumber AD components, even if every AD dimerizes with DBD at high Ca^{2+}, the empty DBDs will still compete with transcriptionally active dimers at the genomic binding site, thereby suppressing TRIC signal in a dominant-negative manner. We validated this intuition through a computational simulation (Online Methods) and observed that, although TRIC signal was monotonically increased by increasing the expression of AD, the signal was first increased and then decreased by increasing DBD expression (**Fig. 4b**). To experimentally test this idea, we constructed *UAS-MKII::nlsLexADBDo* flies, and expressed this transgene in the PI cells with *ilp2-GeneSwitch*, a GAL4-progesterone-receptor fusion protein whose activity can be adjusted using RU486 (ref. 32) (**Supplementary Fig. 5e**). The *in vivo* TRIC signal indeed increased and then decreased as RU486 induction increased (**Fig. 4c**).

Given that DBD/AD stoichiometry was not well controlled when we used the *nsyb* enhancer to express DBD and GAL4/UAS to express AD, we examined NPF neurons as a test for the more balanced expression of both components by GAL4/UAS. TRIC signal was still present in the four neurons originally labeled, albeit at lower levels (**Fig. 4a**,**d**); additional signal emerged in the fan-shaped body (**Fig. 4d**), a brain region that has been implicated in courtship conditioning[33]. Based on the simulation, we next added one copy of the AD transgene, which indeed yielded stronger TRIC signal (**Fig. 4e**). Previous studies have demonstrated that sexual deprivation reduces NPF expression[34], but whether such reduction coincides with diminished activity in NPF neurons is unknown. Using TRIC, we observed that sexual deprivation significantly reduced TRIC labeling in an upper layer of the fan-shaped body ($P = 0.0033$; **Fig. 4f**). Thus, TRIC can also be used to identify changes in neural activity associated with ethologically relevant social experience.

TRIC monitors activity in the PI cells

We next focused on the PI cells, one of the most extensively studied modulatory centers in flies. Given that PI cells regulate extremely diverse physiological and behavioral processes[17], understanding how these cells integrate relevant cues is important. However, the regulation of PI activity is only partially understood (**Fig. 5a**), mostly reliant on immunostaining assays that measure the somatic retention of insulin-like peptides (Ilps)[17]. We therefore examined whether TRIC can detect known regulatory mechanisms affecting PI activity.

With no basal signal (data not shown), robust TRIC signal in the PI cells of pan-neuronal TRIC adults was detected within 1 d of QA induction (**Fig. 1d**), providing temporal control for measuring PI activity. TRIC signals overlapped with Ilp2 (**Fig. 5b**) in flies grown

© 2015 Nature America, Inc. All rights reserved.

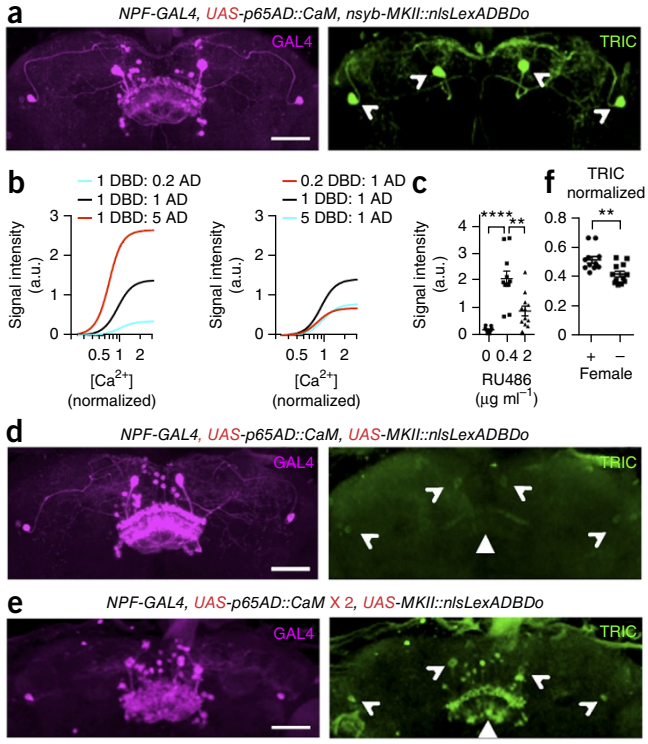

Figure 4 Stoichiometric tuning of TRIC and its application in NPF neurons. (**a**) Monitoring NPF neurons using LexA-based TRIC (*nsyb-MKII::nlsLexADBDo*, *UAS-p65AD::CaM*, *npf-GAL4*, *UAS-mCD8::RFP*, *LexAop2-mCD8::GFP*, representative of ≥6 samples). The GAL4 expression was visualized with RFP (left); the arrowheads indicate the only four cells with prominent TRIC signal (right). (**b**) Simulating effects of DBD/AD stoichiometry on TRIC signal. Increasing AD dose increased signal (left), whereas increasing DBD dose first increased and then decreased signal (right). (**c**) Validation of the scenario in **b** with PI cells (*UAS-MKII::nlsLexADBDo*, *ilp2-GeneSwitch*, *QUAS-p65AD::CaM*, *nsyb-QF2*, *tubP-QS*, *UAS-mCD8::RFP*, *LexAop2-mCD8::GFP*, $n \geq 11$). Increasing GeneSwitch-mediated DBD expression with RU486 first increased and then decreased TRIC signal. Data are presented as mean ± s.e.m. (**d**,**e**) Tuning NPF TRIC signal with more balanced expression of DBD/AD (*UAS-MKII::nlsLexADBDo*, *UAS-p65AD::CaM* [×1 in **d**, ×2 in **e**], *npf-GAL4*, *UAS-mCD8::RFP*, *LexAop2-mCD8::GFP*, representative of ≥6 samples). The arrowheads indicate the same cells as in **a**, and the triangles indicate the additional signal in the fan-shaped body. (**f**) Ratiometric TRIC measurement revealed that sexual deprivation lowered Ca^{2+} activity in male NPF neurons in the fan-shaped body ($n \geq 12$, same genotype as in **e**). Two-tailed unpaired *t* test for **c** ($P < 0.0001$, $P = 0.0022$) and **f** ($P = 0.0033$), with Holm-Bonferroni correction for multiple comparisons. Scale bars in all panels represent 50 μm. $^{**}P < 0.01$, $^{****}P < 0.0001$. Key changes of genetic components are colored red.

on standard food, validating the identity of these cells. Furthermore, the strength of the TRIC signal negatively correlated with Ilp2 levels in individual PI cells (**Fig. 5b**), consistent with the expectation that higher secretory activity leads to less somatic retention of Ilps.

After tuning TRIC expression level (**Fig. 5c** and **Supplementary Fig. 6a**), we found that starvation diminished TRIC signal (**Fig. 5c**), consistent with the reported PI response to nutrients[35,36]. As expected, PI activity was also reduced by deleting *upd2* (**Fig. 5c**), the fly homolog

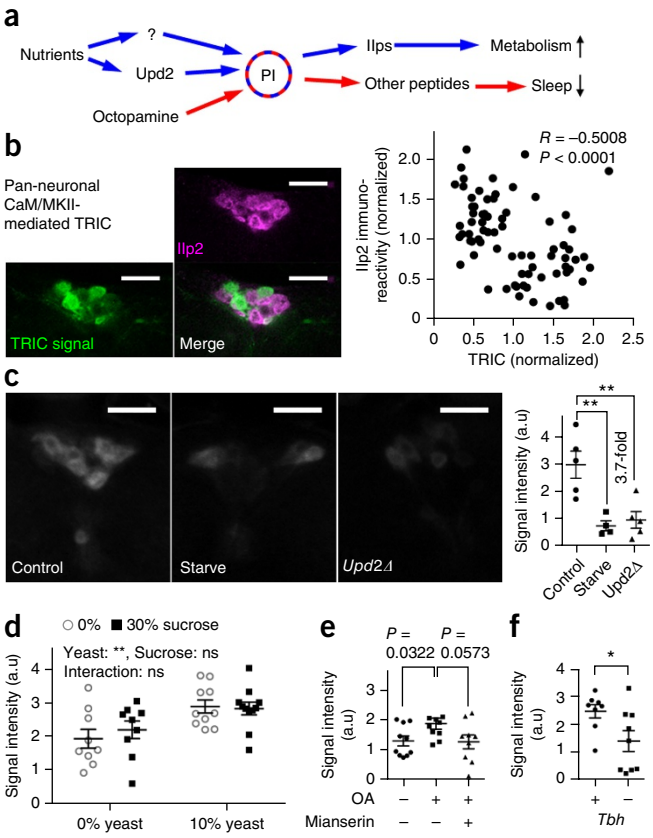

of the hormone leptin that relays a satiety signal from the fat body to the brain[35,36].

Larval PI cells respond to dietary amino acids, but not to sugars[35], and a similar specificity has not been established in adults. To investigate this, we measured TRIC signals after feeding flies with various combinations of yeast and sucrose. We found that yeast increased the TRIC signal in PI cells, whereas sucrose had no effect either by itself or in combination with yeast (**Fig. 5d**), consistent with results in larvae. Given that sucrose, but not amino acid, induces *upd2* expression[36], we reasoned that *upd2* might not be the sole satiety signal. Indeed, starvation reduced the TRIC signal in PI neurons even in *upd2* mutant flies (**Supplementary Fig. 6b**), implying the presence of at least one additional pathway that links satiety to PI activity.

PI cells are also activated by octopamine (OA), a neurotransmitter controlling arousal states[37,38]. We validated that OA feeding increased TRIC signal in PI cells and that an OA antagonist, mianserin, reversed

Figure 5 Monitoring PI cell activity with TRIC. (**a**) Summary of two known pathways regulating PI activity. Our data suggest an unknown pathway in parallel with Upd2 from nutrients to PI. (**b**) TRIC signal in the PI cells negatively correlated with the intensity of Ilp2 staining. Shown are single confocal slices. Spearman's rank correlation for the quantification, where each dot represents one cell after normalizing it to the mean value in the corresponding animal. (**c**) Compared with wild-type flies on regular food (control), TRIC signal in the PI was reduced by food deprivation (starve) or hemizygous *upd2* deletion ($n \geq 4$). 20 mg QA per vial was used to induce TRIC expression. (**d**) Yeast, but not sucrose, increased TRIC signal ($n \geq 8$). (**e**) 10 mg ml^{-1} OA increased TRIC signal, which is antagonized by 2 mg ml^{-1} mianserin, an OA antagonist ($n \geq 9$). (**f**) TRIC signal was reduced by hemizygous *tbh* mutation, which eliminated an enzyme necessary for OA synthesis ($n \geq 8$). All panels are of the same genotype shown in **Figure 1d**, except for **c** and **f**, where *mCD8::RFP* was replaced with *mCD8::GFP*. Two-tailed unpaired *t* test for **c** ($P = 0.0041$, 0.0057), **e** ($P = 0.0032$, 0.0573) and **f** ($P = 0.0313$), with Holm-Bonferroni correction for multiple comparisons. Two-way ANOVA for **d**. Scale bars represent 20 μm. $^{*}P < 0.05$, $^{**}P < 0.01$. Key changes of genetic components are colored red. Data are presented as mean ± s.e.m.

© 2015 Nature America, Inc. All rights reserved.

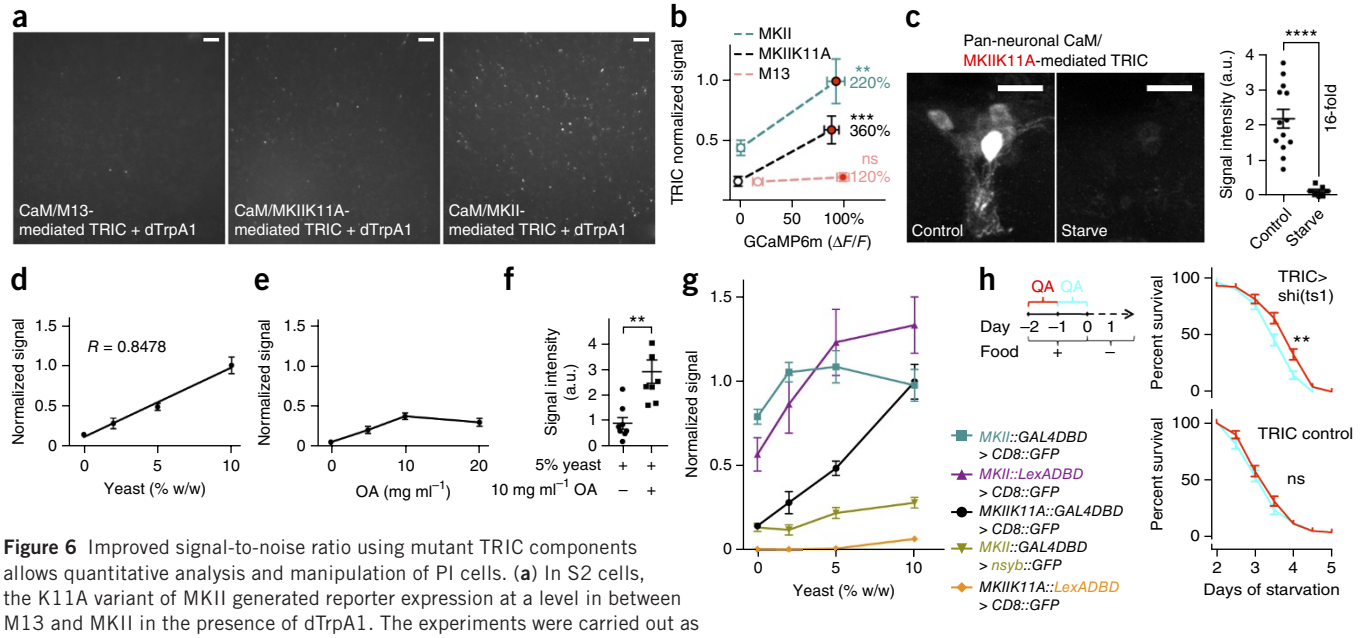

Figure 6 Improved signal-to-noise ratio using mutant TRIC components allows quantitative analysis and manipulation of PI cells. (**a**) In S2 cells, the K11A variant of MKII generated reporter expression at a level in between M13 and MKII in the presence of dTrpA1. The experiments were carried out as described in **Figure 1b**, except for the specific CaM-target peptides. Scale bars represent 50 µm. (**b**) Simultaneous quantification of TRIC and GCaMP6m signals in S2 cells in the presence (red-filled circles) or absence (open circles) of dTrpA1. TRIC normalized signal is the fluorescent intensity of tdTomato expressed by TRIC divided by the baseline fluorescent intensity of GCaMP6m. Of the three variants, MKIIK11A showed the largest fold of TRIC signal induction ($n \geq 189$ cells for each condition). The fold of TRIC signal induction in experimental conditions (with dTrpA1) was labeled in percentage of control (no dTrpA1), as a direct comparison to the scale of $\Delta F/F$. (**c**) TRIC signal showed higher fed-to-starved ratio with MKIIK11A ($n \geq 7$, compared with **Fig. 5c**). (**d**) TRIC signal varied linearly with yeast concentration ($n \geq 9$), showing the Pearson correlation between yeast concentration and the mean TRIC signal at every concentration. (**e**) TRIC signal plateaued as OA concentration increased ($n \geq 9$). (**f**) In the presence of 5% yeast, 10 mg ml^{-1} OA further increased TRIC signal ($n \geq 8$). (**g**) Signals of different TRIC variants in response to varying yeast concentrations ($n \geq 10$ for each data point). All data were normalized to the signal of MKIIK11A::GAL4DBDo driving mCD8::GFP, exposed to 10% yeast; MKIIK11A::GAL4DBDo data were re-plotted from **d**. (**h**) Left, experimental setup. Under the experimental (red) or control (cyan) condition, flies were treated with QA 1–2 or 0–1 d before the onset of starvation (at day 0). Top right, flies with PI activity–dependent expression of *shi*^{ts1} using TRIC (TRIC > *shi*^{ts1}) had extended longevity during starvation in the experimental condition (red) compared with control condition (cyan) (upper panel, $n \geq 94$ flies). Bottom right, flies with TRIC transgenes without *shi*^{ts1} did not exhibit a difference between the experimental and control conditions (lower panel, $n \geq 96$ flies). Base genotype (**c**–**f**): *nsyb-MKIIK11A::GAL4DBDo, QUAS-p65AD::CaM, nsyb-QF2, tubP-QS, UAS-mCD8::RFP/GFP*; **g**: colored components were used to replace corresponding transgene the base genotype; **h**: *mCD8::GFP* in the base genotype was replaced with *shi*^{ts1}. Two-tailed unpaired *t* test for **b** ($P = 0.005$, 0.0005, 0.4114), **c** ($P < 0.0001$) and **f** ($P = 0.0072$) with Holm-Bonferroni correction for multiple comparisons. Log-rank test for **h** ($P = 0.0012$, 0.3411). Scale bars in **c** represent 20 µm. $^{**}P < 0.01$, $^{***}P < 0.001$, $^{****}P < 0.0001$. Key changes of genetic components are colored red. Data are presented as mean ± s.e.m.

© 2015 Nature America, Inc. All rights reserved.

this effect (**Fig. 5e**). As expected, a null allele of *tyramine β hydroxylase* (*tbh*)[39], the gene necessary for OA synthesis, also decreased PI activity (**Fig. 5f**).

In summary, using TRIC, we corroborated regulations of PI activity inferred in previous studies. We also uncovered new information regarding the nutritional requirements for PI activity in adults, and our findings suggest that signaling pathways other than Upd2/leptin also mediate the PI response to satiety (**Fig. 5a**).

Enhancing the dynamic range of TRIC through mutagenesis

Although we validated TRIC in PI cells, the small effect sizes (**Fig. 5d**,**e**) might limit further quantitative analysis. To optimize TRIC, we screened every alanine variant of MKII in S2 cells. Given that the signal of M13 *in vivo* was too low and the baseline of MKII too high, we reasoned that the useful variants would show signals intermediate between M13 and MKII in the presence of dTrpA1 (**Fig. 6a** and data not shown). To examine the relation between TRIC signal and Ca^{2+} concentration, we simultaneously measured the intensity of the fluorescent Ca^{2+} indicator GCaMP6m[40] and a *UAS-tdTomato* reporter expressed by TRIC (Online Methods). dTrpA1-mediated Ca^{2+} influx induced a $\Delta F/F$ of about 100% (**Fig. 6b** and data not shown), comparable to *in vivo* physiological responses[40]. Compared with the no-dTrpA1 control, TRIC signal underwent a 2.2-fold increase with the original MKII, whereas M13 resulted in a signal too weak to be significant ($P = 0.41$; **Fig. 6b**). As an example for the alanine mutants, MKIIK11A reduced both the baseline and the induced TRIC signals compared with MKII, but increased the fold of induction to 3.6 (**Fig. 6b**).

To better understand the behavior of the MKIIK11A variant, we estimated its affinity to CaM based on *in silico* alanine scan (**Supplementary Fig. 7d** and Online Methods) and then simulated its dose response. In the simulation, MKIIK11A lowered the TRIC signal (**Supplementary Fig. 7a**), although the MKII and MKIIK11A dose-response curves were almost identical after normalizing to their respective maximums (**Supplementary Fig. 7a**). Thus, reduced affinity alone was insufficient to account for the increased induction ratio (**Fig. 6b**), unless some form of nonlinearity transformed the proportional decrease of signal by K11A. One possible source of nonlinearity is competition from endogenous CaM and its target peptides. Assuming the simplest case that endogenous CaM and its target peptides are expressed in equal concentrations, and that the endogenous peptides have the same affinity for CaM as MKII, simulation revealed that TRIC signal decreased as the number of endogenous competitors increased (**Supplementary Fig. 7b**), which again preserved the shape of the curve (**Supplementary Fig. 7b**). However, when the K11A variant was simulated in the presence of competition, the mutation caused a rightward shift of the response curve (**Supplementary Fig. 7c**),

consistent with the lower sensitivity and higher induction rate of this variant than MKII. This likely explains the performance of the alanine variant and suggests a mechanism to account for heterogeneity of TRIC efficiency in different neuronal types.

On the basis of our *in vitro* and *in silico* analyses, we tested five intermediate variants in PI cells (data not shown). Of these, MKIIK11A reduced PI TRIC signal in both fed and starved flies, with a larger effect on the latter. Consequently, although the TRIC signal was still robust in fed flies, it was negligible after starvation (**Fig. 6c**), and the ratio of TRIC signals between the fed and starved states quadrupled that of the original MKII (**Figs. 5c** and **6c**).

We took advantage of this variant to measure the temporal characteristics of TRIC signal in PI cells using mCD8::RFP as a reporter. Shortening food induction by half reduced the TRIC signal by half (**Supplementary Fig. 6c**), suggesting that the signal accumulates linearly over time. To measure signal perdurance, we either examined the flies immediately after 1-d induction of PI activity by food or starved them for 1 or 2 d before dissection, and found the half-life of the TRIC signal to be 0.55 d (**Supplementary Fig. 6d**).

TRIC reveals distinct modes of PI activity regulation

Signal induction by yeast and OA was also greatly improved by MKIIK11A (**Figs. 5d**,**e** and **Supplementary Fig. 6e**,**f**), which allowed us to quantitatively compare the dose responses in PI neurons to yeast and OA exposure. PI TRIC signal increased linearly with yeast concentration (**Fig. 6d**). In contrast, as the OA concentration rose, the TRIC signal plateaued at a level much lower than the maximal signal induced by yeast (**Fig. 6d**,**e**). One possible explanation for this nonlinear response was that OA uptake was simply saturated. In this scenario, 10 or 20 mg ml^{-1} OA would result in the same amount of OA acting on its receptors in PI cells, and their effects should be equally inhibited by mianserin. To test this, we used an intermediate mianserin dose (**Supplementary Fig. 6g**) and found that 10 mg ml^{-1} OA induced a smaller TRIC signal than 20 mg ml^{-1} OA (**Supplementary Fig. 6g**). Thus, OA uptake was not saturated under these conditions, suggesting that the observed saturation of the TRIC signal took place at or downstream of the OA receptors.

The difference in dose-response curves suggests that yeast and OA activate PI cells through separate pathways. To test this notion, we asked whether the response to 5% yeast, which induced PI activity higher than the ceiling of OA response (**Fig. 6d**,**e**), could be further augmented by adding OA. Indeed, adding 10 mg ml^{-1} OA increased the signal induced by 5% yeast (**Fig. 6f**). In summary, nutrients and OA regulate PI activity through separate pathways and display distinct dose responses.

TRIC variants cover a wide range of neural activity

Our characterization of TRIC thus far contains several variants of TRIC. We used yeast-regulated PI activity to quantitatively compare these variants. All of the subsequent data were normalized to the TRIC signal of MKIIK11A::GAL4DBDo driving mCD8::GFP, exposed to 10% yeast.

Compared with MKIIK11A::GAL4DBDo (**Fig. 6g**), the original MKII::GAL4DBDo driving mCD8::GFP displayed a high baseline with plain agar and was saturated using 2% yeast (**Fig. 6g**). Replacing GAL4DBDo with nlsLexADBDo led to a more gradual elevation of signal as yeast concentration increased (**Fig. 6g**); replacing the mCD8 reporter with nsyb::GFP greatly reduced the signal while also increasing the range of signal induction (**Fig. 6g**). Finally, combining the MKIIK11A mutation with nlsLexADBDo, we detected no TRIC signal except at the highest yeast concentration (10%; **Fig. 6g**). Taken together, these comparisons indicate that MKII::GAL4DBDo driving mCD8::GFP is the most sensitive reporter and MKIIK11A::nlsLexADBDo driving mCD8::GFP is the most stringent. Collectively, these variants display a wide dynamic range that can be selected by users in their neurons of interest.

A TRIC-driven synaptic blocker enhances stress resistance

Having achieved a high signal-to-baseline ratio of the MKIIK11A variant in PI cells, we tested whether TRIC-based expression of an effector can be used to manipulate circuit function. We used TRIC to express *shi^{ts1}*, a widely used mutant dynamin that disrupts synaptic transmission at restrictive temperature[41]. We focused on validating a well-characterized phenotype in which inactivating PI cells enhances stress resistance, as measured by survival following starvation[42].

All *TRIC* > *shi^{ts1}* flies were first kept at 25 °C on food for 2 d. The experimental group (**Fig. 6h**) was exposed to QA on the first day, and *shi^{ts1}* was expressed on the second day in PI cells as a result of food-induced activity; the control group (**Fig. 6h**) was exposed to QA on the second day, and there was minimal PI activity to follow the onset of TRIC and no *shi^{ts1}* expression. All flies were then starved at the restrictive temperature for *shi^{ts1}*. The experimental group survived significantly longer than the control group (P = 0.0012; **Fig. 6h**). Further controls confirmed that there was no difference in survival in the absence of the *shi^{ts1}* transgene (**Fig. 6h**). The phenotype is like a result of expression in PI cells rather than elsewhere in the brain, given that when we visualized TRIC signal in the whole brain under these conditions, the only notable difference between the control and the experiment was in the PI cells (**Supplementary Fig. 6h**). TRIC can therefore mediate neural activity–dependent expression of genetic effectors that manipulate circuit function.

DISCUSSION

Using cultured cells and multiple *in vivo* assays, we found that TRIC reports changes in Ca^{2+} levels under diverse conditions in visual, olfactory and neuromodulatory systems. Our results provide quantitative assessments for choosing TRIC variants with appropriate sensitivity and stringency, and proof of principle that TRIC can be used to express a circuit manipulator. Thus, TRIC acts as a useful complement to functional Ca^{2+} imaging by integrating changes in activity over long periods of time and offering genetic access to neurons on the basis of their activity.

Comparing TRIC with other methods

Vertebrate IEGs, which evolved to be expressed in a high signal-to-baseline ratio in response to neuronal activation, are widely used to report neuronal activity[7]. However, as they rely on endogenous signaling networks, their response properties and cell-type biases are difficult to modify. TRIC can be considered a rationally designed IEG, by exogenously introducing a protein-peptide interaction to detect Ca^{2+}. The modular design of TRIC renders it more amenable to optimization. TRIC reports a rise in nuclear Ca^{2+} levels, which has previously been used to monitor pan-neuronal activity in *C. elegans*[43], and also accompanies neuronal activation in mammalian neurons likely shuttled by Ca^{2+}-binding proteins[44]. Our experiments indicate that nuclear Ca^{2+} correlates with activity in diverse neuronal classes in flies. It is likely that not all cell types have the same efficiency in converting cytoplasmic Ca^{2+} signal to nuclear Ca^{2+} signal. Thus, TRIC efficiency and optimization may differ for different neuronal types.

While this manuscript was in review, a Ca^{2+} integrator (CaMPARI) was reported in which the ultraviolet conversion of emission spectrum of a fluorescent protein was engineered to be contingent on

© 2015 Nature America, Inc. All rights reserved.

Ca^{2+} concentration[45]. CaMPARI can capture neuronal activity on a shorter time scale than TRIC or IEG. However, access of neurons to ultraviolet may limit the use of CaMPARI in deep tissues, at least in large animals, whereas TRIC and IEG report neuronal activity in the entire nervous system non-invasively. Notably, unlike CaMPARI or IEG, TRIC offers genetic access to active neurons, allowing activity-based circuit manipulation (**Fig. 6h**).

Tuning the parameters of TRIC

Our results underscore the importance of optimizing TRIC for specific neuronal types. In this study, we have optimized TRIC for multiple cell types, and have described many variants that can help users in other cells (**Fig. 6g** and **Supplementary Table 2**). We recommend that users begin with CaM/MKII-mediated TRIC (**Figs. 1**, **5** and **6g**) in their neurons of interest. If TRIC signal is detected, the users can attempt QA-mediated (**Figs. 5** and **6**) or FLP-mediated (**Fig. 2**) regulation of the timing of TRIC onset. The signal-to-baseline ratio can be further improved by titrating expression of TRIC using QA (**Fig. 5** and **Supplementary Fig. 6**), choosing reporters with different stabilities (**Figs. 3** and **6g**, and **Supplementary Fig. 2**), or switching to nlsLexADBDo (**Figs. 3** and **6g**) or the MKIIK11A variant (**Fig. 6** and **Supplementary Fig. 6**). Stoichiometry can also be leveraged to boost TRIC signal (**Fig. 4**).

With the current version of TRIC, the signal accumulates and decays over many hours (**Supplementary Fig. 6c**,**d**). To detect shorter periods of neuronal activity, an important future goal is to increase signal strength while avoiding saturation by basal Ca^{2+} concentrations. One solution to this problem would be to restrict TRIC to a narrower time window than that offered by the QA- or the FLP-mediated strategy. For example, TRIC could be split into DBD-X, Y–target peptide and CaM-AD, where X and Y are two interacting modules controlled by light[46]. One could then synchronize TRIC with a specific manipulation, or even trigger TRIC repetitively with specific behavioral features using feedback from automated tracking[47]. To preserve phasic information about neuronal activity, reporters with faster decays than CD8::GFP (**Supplementary Fig. 2c**) could be used or the TRIC components could be destabilized with tags for protein degradation. Given that the current TRIC was able to interact with endogenous CaM and its target peptides, another important direction is to 'isolate' TRIC by co-engineering the CaM and MKII components to lose binding to their endogenous partners, but maintain their mutual interaction[48]. Future TRIC optimization could be achieved using high throughput screens in cultured cells, which can predict *in vivo* performance (**Figs. 1**, **5** and **6**, and **Supplementary Fig. 1**).

The modulation of PI activity

Previous studies[17,35,36] used Ilp2 immunostaining, epitope-tagged Ilp2 or a secreted GFP as indirect indicators of PI activity. We validated the major conclusions of these studies using TRIC. After enhancing the dynamic range of TRIC, we gained additional insight into how PI activity is regulated. In particular, given that PI cells affect diverse processes, how do these cells determine their output according to all relevant inputs? For example, an animal may encounter conflicting metabolic needs, such as conserving energy versus defending territory in an impoverished environment. Our nutrient and OA comparison could be viewed as a minimal model of such a dilemma, as OA contributes to arousal and is necessary for 'fight or flight' in insects[38,49]. We found that PI cells exhibited graded, yet more readily saturated, responses to such events. In contrast, the linear PI response to nutrients extended over a wider range. These distinctions, as well as the additive interaction between yeast and OA, point to the independent operation of these two categories of inputs. To further survey the input landscape, one could genetically manipulate candidate receptors autonomously or candidate upstream neurons non-autonomously while monitoring PI activity using TRIC.

Applying TRIC to other systems

The physiological states of flies can change over hours to days and can be accompanied by changes in the activities of neurons expressing modulatory neurotransmitters[3,4] or neuropeptides[17,34]. Although previous work has focused on the targets of modulatory neurotransmitters, inputs to these cells remain largely unknown. In addition, there are ~75 predicted neuropeptides in flies, only a small subset of which have been examined[50]. TRIC can be applied to neurons expressing specific transmitters or neuropeptides and tested in different physiological states (for example, the NPF neurons in **Fig. 4**). We note that the current TRIC variants might not fit the dynamic range of all neuronal types, and it might be necessary to test other AD/DBD ratios or other MKII mutants following our examples of optimization for PI cells.

Finally, TRIC can report a rise of intracellular Ca^{2+} that accompanies any cellular, developmental or physiological processes in flies and can be adapted for similar use in other model organisms. TRIC modules can be introduced as transgenes or by viral vectors, and specific stoichiometry can be achieved by specifying the number of AD and DBD sequences in multi-cistronic constructs. TRIC expression can be made contingent on recombinase or other binary systems in model organisms, such as mice, where many Cre lines are available for spatiotemporal control, which can help refine activity monitoring and circuit manipulation in specific cell types.

METHODS

Methods and any associated references are available in the online version of the paper.

Accession codes. Addgene: pActP-dtrpA1, 64713; pActP-GCaMP6m, 64714; pQUAST-p65AD::CaM, 64715; pQUAST-frt-stop-frt-p65AD::CaM, 64716; pUASTattB-p65AD::CaM, 64717; pUASTattB-MKII::nlsLexADBDo, 64718; pBP-p65AD::CaM, 64719; pattB-nsyb-M13::GAL4DBDo, 64720; pattB-nsyb-MKII::GAL4DBDo, 64721; pattB-nsyb-MKIIK11A::GAL4DBDo, 64722; pQUAST-MKII::GAL4DBDo, 64723; pQUAST-M13::GAL4DBDo, 64724; pattB-nsyb-MKII::nlsLexADBDo, 64725; pattB-nsyb-MKIIK11A::nlsLexADBDo, 64726.

Note: Any Supplementary Information and Source Data files are available in the online version of the paper.

ACKNOWLEDGMENTS

We thank D. Luginbuhl (Stanford University) for generating transgenic flies, R. Alfa, J. Cao, X. Dong, Y. Fisher, D.M. Gohl, M. Lin, S. Park, C. Ran, K. Shen, M. Silies, X. Wei, Z. Yang and C. Zhou for advice and technical support, H.A. Dierick (Baylor College of Medicine), G. Dietzl (Stanford University), T. Lee (Janelia Farm), A. Rajan (Harvard University), G.M. Rubin (Janelia Farm), J.W. Wang (University of California, San Diego), M. Zeidler (University of Sheffield) and Bloomington Stock Center for fly strains, Addgene for plasmids, and L. DeNardo Wilke, C.J. Guenthner, T.J. Mosca and X. Wang for critiques on the manuscript. X.J.G. is supported by an Enlight Foundation Interdisciplinary Fellowship. L.L. receives funding from the Howard Hughes Medical Institute. This study was also supported by US National Institutes of Health grants R01-DC005982 (L.L.), R01-EY022638 (T.R.C.) and R01-DC013070 (C.J.P.), and a grant from Whitehall Foundation (C.J.P.).

AUTHOR CONTRIBUTIONS

X.J.G. designed, performed and analyzed the experiments, aided by J.L. during revision. L.L. and T.R.C. supervised the project. O.R. and C.J.P. provided the unpublished *nsyb-QF2* line. X.J.G., L.L. and T.R.C. wrote the manuscript, with inputs from the other authors.

© 2015 Nature America, Inc. All rights reserved.

COMPETING FINANCIAL INTERESTS

The authors declare no competing financial interests.

Reprints and permissions information is available online at http://www.nature.com/reprints/index.html.

1. Tsien, R.Y. Fluorescence measurement and photochemical manipulation of cytosolic free calcium. *Trends Neurosci.* **11**, 419–424 (1988).
2. Looger, L.L. & Griesbeck, O. Genetically encoded neural activity indicators. *Curr. Opin. Neurobiol.* **22**, 18–23 (2012).
3. Marella, S., Mann, K. & Scott, K. Dopaminergic modulation of sucrose acceptance behavior in *Drosophila*. *Neuron* **73**, 941–950 (2012).
4. Inagaki, H.K. *et al.* Visualizing neuromodulation *in vivo*: TANGO-mapping of dopamine signaling reveals appetite control of sugar sensing. *Cell* **148**, 583–595 (2012).
5. Nusbaum, M.P., Blitz, D.M., Swensen, A.M., Wood, D. & Marder, E. The roles of co-transmission in neural network modulation. *Trends Neurosci.* **24**, 146–154 (2001).
6. Takemura, S.Y. *et al.* A visual motion detection circuit suggested by *Drosophila* connectomics. *Nature* **500**, 175–181 (2013).
7. Sheng, M. & Greenberg, M.E. The regulation and function of c-fos and other immediate early genes in the nervous system. *Neuron* **4**, 477–485 (1990).
8. Reijmers, L.G., Perkins, B.L., Matsuo, N. & Mayford, M. Localization of a stable neural correlate of associative memory. *Science* **317**, 1230–1233 (2007).
9. Koya, E. *et al.* Targeted disruption of cocaine-activated nucleus accumbens neurons prevents context-specific sensitization. *Nat. Neurosci.* **12**, 1069–1073 (2009).
10. Guenthner, C.J., Miyamichi, K., Yang, H.H., Heller, H.C. & Luo, L. Permanent genetic access to transiently active neurons via TRAP: targeted recombination in active populations. *Neuron* **78**, 773–784 (2013).
11. Kawashima, T. *et al.* Functional labeling of neurons and their projections using the synthetic activity-dependent promoter E-SARE. *Nat. Methods* **10**, 889–895 (2013).
12. Fujita, N. et al. Visualization of neural activity in insect brains using a conserved immediate early gene, Hr38. *Curr. Biol.* **23**, 2063–2070 (2013).
13. Masuyama, K., Zhang, Y., Rao, Y. & Wang, J.W. Mapping neural circuits with activity-dependent nuclear import of a transcription factor. *J. Neurogenet.* **26**, 89–102 (2012).
14. Rhoads, A.R. & Friedberg, F. Sequence motifs for calmodulin recognition. *FASEB J.* **11**, 331–340 (1997).
15. Luan, H., Peabody, N.C., Vinson, C.R. & White, B.H. Refined spatial manipulation of neuronal function by combinatorial restriction of transgene expression. *Neuron* **52**, 425–436 (2006).
16. Pfeiffer, B.D. *et al.* Refinement of tools for targeted gene expression in *Drosophila*. *Genetics* **186**, 735–755 (2010).
17. Nassel, D.R. Insulin-producing cells and their regulation in physiology and behavior of *Drosophila*. *Can. J. Zool.* **90**, 476–488 (2012).
18. Hamada, F.N. *et al.* An internal thermal sensor controlling temperature preference in *Drosophila*. *Nature* **454**, 217–220 (2008).
19. Peersen, O.B., Madsen, T.S. & Falke, J.J. Intermolecular tuning of calmodulin by target peptides and proteins: differential effects on Ca^{2+} binding and implications for kinase activation. *Protein Sci.* **6**, 794–807 (1997).
20. Potter, C.J., Tasic, B., Russler, E.V., Liang, L. & Luo, L. The Q system: a repressible binary system for transgene expression, lineage tracing, and mosaic analysis. *Cell* **141**, 536–548 (2010).
21. Riabinina, O. *et al.* Improved and expanded Q-system reagents for genetic manipulations. *Nat. Methods* **12**, 219–222 (2015).
22. Bloomquist, B.T. *et al.* Isolation of a putative phospholipase C gene of *Drosophila*, norpA, and its role in phototransduction. *Cell* **54**, 723–733 (1988).
23. Estes, P.S., Ho, G.L.Y., Narayanan, R. & Ramaswami, M. Synaptic localization and restricted diffusion of a *Drosophila* neuronal synaptobrevin—green fluorescent protein chimera *in vivo*. *J. Neurogenet.* **13**, 233–255 (2000).
24. Wong, A.M., Wang, J.W. & Axel, R. Spatial representation of the glomerular map in the *Drosophila* protocerebrum. *Cell* **109**, 229–241 (2002).
25. Clark, D.A., Bursztyn, L., Horowitz, M.A., Schnitzer, M.J. & Clandinin, T.R. Defining the computational structure of the motion detector in *Drosophila*. *Neuron* **70**, 1165–1177 (2011).
26. Gaudry, Q., Hong, E.J., Kain, J., de Bivort, B.L. & Wilson, R.I. Asymmetric neurotransmitter release enables rapid odor lateralization in *Drosophila*. *Nature* **493**, 424–428 (2013).
27. Friggi-Grelin, F. *et al.* Targeted gene expression in *Drosophila* dopaminergic cells using regulatory sequences from tyrosine hydroxylase. *J. Neurobiol.* **54**, 618–627 (2003).
28. Alekseyenko, O.V., Lee, C. & Kravitz, E.A. Targeted manipulation of serotonergic neurotransmission affects the escalation of aggression in adult male *Drosophila melanogaster*. *PLoS ONE* **5**, e10806 (2010).
29. Cole, S.H. *et al.* Two functional but noncomplementing *Drosophila* tyrosine decarboxylase genes. *J. Biol. Chem.* **280**, 14948–14955 (2005).
30. Wu, Q. *et al.* Developmental control of foraging and social behavior by the *Drosophila* neuropeptide Y-like system. *Neuron* **39**, 147–161 (2003).
31. Park, D., Veenstra, J.A., Park, J.H. & Taghert, P.H. Mapping peptidergic cells in *Drosophila*: where DIMM fits in. *PLoS ONE* **3**, e1896 (2008).
32. Fridell, Y.W., Sanchez-Blanco, A., Silvia, B.A. & Helfand, S.L. Targeted expression of the human uncoupling protein 2 (hUCP2) to adult neurons extends life span in the fly. *Cell Metab.* **1**, 145–152 (2005).
33. Joiner, M.A. & Griffith, L.C. Mapping of the anatomical circuit of CaM kinase–dependent courtship conditioning in *Drosophila*. *Learn. Mem.* **6**, 177–192 (1999).
34. Shohat-Ophir, G., Kaun, K.R., Azanchi, R., Mohammed, H. & Heberlein, U. Sexual deprivation increases ethanol intake in *Drosophila*. *Science* **335**, 1351–1355 (2012).
35. Géminard, C., Rulifson, E.J. & Leopold, P. Remote control of insulin secretion by fat cells in *Drosophila*. *Cell Metab.* **10**, 199–207 (2009).
36. Rajan, A. & Perrimon, N. *Drosophila* cytokine unpaired 2 regulates physiological homeostasis by remotely controlling insulin secretion. *Cell* **151**, 123–137 (2012).
37. Crocker, A., Shahidullah, M., Levitan, I.B. & Sehgal, A. Identification of a neural circuit that underlies the effects of octopamine on sleep:wake behavior. *Neuron* **65**, 670–681 (2010).
38. Roeder, T. Tyramine and octopamine: Ruling behavior and metabolism. *Annu. Rev. Entomol.* **50**, 447–477 (2005).
39. Monastirioti, M., Linn, C.E. Jr. & White, K. Characterization of *Drosophila* tyramine beta-hydroxylase gene and isolation of mutant flies lacking octopamine. *J. Neurosci.* **16**, 3900–3911 (1996).
40. Chen, T.W. *et al.* Ultrasensitive fluorescent proteins for imaging neuronal activity. *Nature* **499**, 295–300 (2013).
41. Kitamoto, T. Conditional modification of behavior in *Drosophila* by targeted expression of a temperature-sensitive shibire allele in defined neurons. *J. Neurobiol.* **47**, 81–92 (2001).
42. Broughton, S.J. *et al.* Longer lifespan, altered metabolism, and stress resistance in *Drosophila* from ablation of cells making insulin-like ligands. *Proc. Natl. Acad. Sci. USA* **102**, 3105–3110 (2005).
43. Schrödel, T., Prevedel, R., Aumayr, K., Zimmer, M. & Vaziri, A. Brain-wide 3D imaging of neuronal activity in *Caenorhabditis elegans* with sculpted light. *Nat. Methods* **10**, 1013–1020 (2013).
44. Ma, H. *et al.* gammaCaMKII shuttles Ca(2)(+)/CaM to the nucleus to trigger CREB phosphorylation and gene expression. *Cell* **159**, 281–294 (2014).
45. Fosque, B.F. *et al.* Neural circuits. Labeling of active neural circuits *in vivo* with designed calcium integrators. *Science* **347**, 755–760 (2015).
46. Schmidt, D. & Cho, Y.K. Natural photoreceptors and their application to synthetic biology. *Trends Biotechnol.* **33**, 80–91 (2015).
47. Bath, D.E. *et al.* FlyMAD: rapid thermogenetic control of neuronal activity in freely walking *Drosophila*. *Nat. Methods* **11**, 756–762 (2014).
48. Palmer, A.E. *et al.* Ca^{2+} indicators based on computationally redesigned calmodulin-peptide pairs. *Chem. Biol.* **13**, 521–530 (2006).
49. Zhou, C., Rao, Y. & Rao, Y. A subset of octopaminergic neurons are important for *Drosophila* aggression. *Nat. Neurosci.* **11**, 1059–1067 (2008).
50. Nässel, D.R. & Winther, A.M. *Drosophila* neuropeptides in regulation of physiology and behavior. *Prog. Neurobiol.* **92**, 42–104 (2010).

© 2015 Nature America, Inc. All rights reserved.

ONLINE METHODS

Recombinant DNA construction. DNA construction was made using standard cloning methods. PCR amplifications were conducted with high-fidelity Phusion polymerase (NEB #M0535). The insertions were all verified by sequencing. Several intermediate constructs were not referred to in the paper.

pAC-dTrpA1. The *dTrpA1* sequence was amplified from *pUAST-dTrpA1* (ref. 18) using primers CGATGCGGCCGCAACATGACTTCGGGCGACA and CGATGGCGCGCCTACATGCTCTTATTGAAGCTCAGG, and cloned into pP_{AC5C}-PL[15] using NotI/AscI.

pAC-GCaMP6m. The GCaMP sequence was amplified using primers ATCCG ATCTGCGGCCGCAAAATGGGTTCTCATCATCATCA and ATCGGTTATG GCGCGCCTCACTTCGCTGTCATCATT, and cloned into NotI/AscI-digested pP_{AC5C}-PL using In-Fusion reaction (Clontech #638910).

pAC-VP16AD::CaM. The *CaM* sequence was amplified from GCaMP3 (ref. 51) using primers CGATACTAGTGACCAACTGACTGAAGAGCAGATCG and CGATGGCGCGCCTTACTTCGCTGTCATCATTTGTACAAACTCT, replacing the leucine zipper in *pAC-VP16AD::Zp*[15] using SpeI/AscI.

pAC-p65AD::CaM. The *p65AD* sequence was amplified from *pBP-p65ADZpUw*[16] using primers CGATGCGGCCGCAAAACATGGATAAAGCG GAATTAATTCC and CTCCGCTAGCGGAGCTTATCT, replacing the *VP16AD* in *pAC-VP16AD::CaM* using NotI/NheI.

pAC-M13::GAL4DBD. The *M13* sequence was amplified from GCaMP3 (ref. 51) using primers CGATGCGGCCGCCACCATGGGTTCTCATCA and CGATTCTAGATGAGCTCAGCCGACCTATAGCT, digested with NotI/XbaI, and used to replace the leucine zipper in *pAC-Zp::GAL4DBD*[15] between NotI/NheI.

pAC-M13::GAL4DBDo. The *GAL4DBDo* (codon-optimized) sequence was amplified from *pBPZpGAL4DBDUw*[16] using primers GGAGGTACTAGTATGA AGCTGCTGAG and CGATGGCGCGCCTTACGATACCGTCAGTTGCCGT, replacing the *GAL4DBD* in *pAC-M13::GAL4DBDo* using SpeI/AscI.

pAC-MKII::GAL4DBD. The *MKII* (codon-optimized) sequence[19] was generated by annealing oligos GGCCGCCACCATGTTTAATGCGCGGCGCAAGCT AAAGGGAGCCATACTTACGACAATGTTGGCGACCAGAAATTTTTCGG and CTAGCCGAAAAATTTCTGGTCGCCAACATTGTCGTAAGTATGGCT CCCTTTAGCTTGCGCCGCGCATTAAACATGGTGGC, and ligated between the NotI/NheI sites on *pAC-Zp::GAL4DBD* to replace *Zp*.

pAC-skMLCKN5A::GAL4DBD. The *skMLCKN5A* (codon-optimized) sequence[19] was generated by annealing oligos GGCCGCCACCATGGGCCGC TGGAAGAAGGCCTTCATCGCCGTGAGCGCCGCCAACCGCTTCAAGA AGATCAGCG and CTAGCGCTGATCTTCTTGAAGCGGTTGGCGGCGCT CACGGCGATGAAGGCCTTCTTCCAGCGGCCCATGGTGGC, and ligated between the NotI/NheI sites on *pAC-Zp::GAL4DBD* to replace *Zp*. We chose the N5A mutation that increases CaM-skMLCK affinity[52].

pAC-MKII::GAL4DBDo. The *GAL4DBDo* (codon-optimized) sequence was amplified from *pBPZpGAL4DBDUw*[16] using primers GGAGGTACTAGTATGA AGCTGCTGAG and CGATGGCGCGCCTTACGATACCGTCAGTTGCCGT, replacing the *GAL4DBD* in *pAC-MKII::GAL4DBDo* using SpeI/AscI.

Alanine variants of *pAC-MKII::GAL4DBDo*. For alanine variant of each residue, the corresponding codon in MKII was changed to GCC. For example, the *MKIIK11A* sequence was generated by annealing oligos GGCCGCCACCATG TTTAATGCGCGGCGCAAGCTAgccGGAGCCATACTTACGACAATGTTGG CGACCAGAAATTTTTCGG and CTAGCCGAAAAATTTCTGGTCGCCAA CATTGTCGTAAGTATGGCTCCggcTAGCTTGCGCCGCGCATTAAACATG GTGGC (the replaced codon in lowercase), replacing the *MKII* in *pAC-MKII::GAL4DBDo* using NotI/NheI.

pQUAST-p65AD::CaM. The *p65AD::CaM* sequence was amplified from *pAC-p65AD::CaM* using primers CGATAGATCTCAACATGGATAAAGCGG AATTAATTCC and CGATCTCGAGTTACTTCGCTGTCATCATTTGTACA AACTCT, and cloned in to *pQUAST*[20] using BglII/XhoI.

pattB-nsyb-M13::GAL4DBDo. The *M13::GAL4DBDo* sequence was amplified from *pAC-M13::GAL4DBDo* using primers CGATGAATTCACCATGGGTTCT CATCATCATCATC and CGATGACGTCTTACGATACCGTCAGTTGCCGT, replacing the *GAL4* in *pattB-nsyb-GAL4*[21] using EcoRI/AatII.

pattB-nsyb-MKII::GAL4DBDo and the alanine variants. The *MKII::GAL4DBDo* sequence was amplified from *pAC-MKII::GAL4DBDo* using primers CGATGAATTCACCATGTTTAATGCGC and CGATGACGTCTTA CGATACCGTCAGTTGCCGT, replacing the *GAL4* in *pattB-nsyb-GAL4* using EcoRI/AatII. For the alanine variants, the corresponding codon in the 5′ primer is changed accordingly.

pQUAST-FRT-stop-FRT-p65AD::CaM. The *FRT-stop-FRT* sequence was amplified from *pQUAST-FRT-stop-FRT-mCD8::GFP*[20] using primers TAACAGATCTGAGGGTACCCG and CGATAGATCTGGTACCCAGCTT CAAAAGC, and cloned into *pQUAST-p65AD::CaM* using BglII. The correct orientation was selected after sequencing.

pAC-MKII::nlsLexADBDo. The *nlsLexADBDo* (codon-optimized) sequence was amplified from *pBPnlsLexA-p65Uw*[16] using primers CGATACTAGTCCACC CAAGAAGAAGCG and CGATGGCGCGCCTTACAGCCAATCTCCGTTGC, replacing the *GAL4DBD* in *pAC-MKII::GAL4DBDo* using SpeI/AscI.

pattB-nsyb-MKII::nlsLexADBDo. The *MKII::nlsLexADBDo* sequence was amplified from *pAC-MKII::nlsLexADBDo* using primers CGATGAATTCAC CATGTTTAATGCGC and CGATGACGTCTTACAGCCAATCTCCGTTGC, replacing the *GAL4* in *pattB-nsyb-GAL4* using EcoRI/AatII.

pattB-nsyb-MKIIK11A::nlsLexADBDo. The *MKII::nlsLexADBDo* sequence with the desired point mutation was amplified from *pattB-nsyb-MKII::nlsLexADBDo* using primers ATCGACAGCCGAATTCACCATGT TTAATGCGCGGCGCAAGCTAGCCGGAGCCATACTTACGACAA and CTTTAGTCGACGGTATCGATAG, and cloned into EcoRI/AatII-digested *pattB-nsyb-GAL4* using In-Fusion reaction.

pUAST-attB-p65AD::CaM. The *p65AD::CaM* sequence was digested from *pQUAST-p65AD::CaM* using EcoRI/XhoI and ligated into the corresponding sites in *pUAST-attB*[53].

pUAST-attB-MKII::nlsLexADBDo. The *MKII::nlsLexADBDo* sequence was amplified from *nsyb-MKII::nlsLexADBDo* using primers ATTCGTTAACAG ATCTCACCATGTTTAATGCGC and TAGAGGTACCCTCGAGTTACAGC CAATCTCCGTTG, and cloned into BglII/XhoI-digested *pUAST-attB*[53] using In-Fusion reaction.

S2 cell transfection, manipulation and quantification. S2 cells were maintained in Schneider's Insect Medium (Sigma #S0146), supplemented with 10% heat inactivated fetal bovine serum (FBS) and antibiotics. The cells were cultured in a 25 °C air incubator. The DNAs for transfection were mini-prepped (Qiagen) and their concentrations were measured with a NanoDrop spectrophotometer (Thermo Scientific). All transfections were performed with Effectene Reagent (Qiagen) following the manufacturer's protocol.

The qualitative images were collected from 96-well plates. For each well, 25 ng of each plasmid was used and supplemented with carrier plasmid so that the total amount of DNA was always 100 ng. The transfected cells were kept in the 25 °C incubator for 12 h, and then transferred onto a thermal cycler (MJ research, #PTC-200). The heat-shock program was 3 s at 35 °C and 27 s at 22 °C without lid heating, repeating for 36 h. The cells were then imaged under a fluorescent microscope using the same parameters.

Quantitative comparisons of Ca^{2+} signals using a fluorescence indicator GCaMP6m and a TRIC reporter tdTomato were performed on chambered cover glasses (Fisher Scientific 12565470) using the adherent S2R+ cells. For each chamber, 15 ng of DBD, 10 ng of AD, 20 ng of UAS-tdTomato, and 75 ng of GCaMP6m plasmids were used; the stimulus conditions involved 30, 15 and 15 ng dTrpA1 plasmid for MKII, MKIIK11A and M13 respectively, supplemented with carrier plasmid so that the total amount of DNA was always 150 ng. The transfected cells were kept in the 25 °C incubator for 8 h, and then transferred onto a thermal cycler with the aforementioned heat-shock program for 18 h. The cells were then imaged on an inverted spinning disk microscope at ~25 °C. For each chamber, we first imaged tdTomato signal in seven randomly selected fields of views. We then imaged GCaMP signal at exactly the same positions for 10 frames at 0.1 Hz, and delivered 200 µl of 45 °C S2 medium to the 200 µl medium already in the chamber to reach approximately 35 °C. The baseline image of GCaMP was the mean of the first five frames; these signals were used to segment the cells with custom Matlab scripts. For each cell, its mean intensity of TRIC signal was normalized to its mean baseline intensity of GCaMP to account for intercellular variability of transfection and expression; the heat-induced peak signal of GCaMP was the highest intensity among the last five frames, and $\Delta F/F$ was calculated as (peak-baseline)/baseline. Each data point represents the mean of all cells from duplicated wells.

© 2015 Nature America, Inc. All rights reserved.

doi:10.1038/nn.4016

Fly husbandry. In addition to the flies generated with standard P element–mediated or site-directed transgenesis for this study (**Supplementary Table 2**), the following flies were used (annotated with Bloomington Stock # when available): *tubP-QS* (30022), *UAS-mCD8::RFP* (32229), *lexAop2-mCD8::GFP* (32229), *UAS-mCD8::GFP* (5137), *norpA*[20] (ref. 22), *UAS-nsyb::GFP* (9263), *UAS-GFP::RpL10A* (42683), *hsFLP* and *UAS>CD2, y+>CD8::GFP*[24], *hsFLP122* (ref. 54), *GH146-QF* (30015), *pebbled-GAL4* (ref. 55), *ey-FLP* (5580), *UAS>w+>RTA*[56], *UAS-luciferase* (gift from G. Dietzl), *GH146-LexA*[57], *LexAop2-dtrpA1* (gift from G. Rubin), *upd2Δ* (ref. 58), *UAS-CaLexA* and *LexAop-mCD8::GFP::2A::mCD8::GFP*[13], *Tbh*^{nM18} (ref. 39), *ple-GAL4* (8848), *trh-GAL4* (38388), *tdc2-GAL4* (9313), *npf-GAL4* (25681), *dimm-GAL4* (25373), *ilp2-GeneSwitch*[32], *orco-GAL4* (26818), *UAS-shi*^{ts1} (ref. 41), *nsyb-QF2* (ref. 21).

We used the cornmeal, molasses and yeast medium listed on Bloomington website. All experimental flies were raised in a dark 25 °C incubator unless specified, and collected 1–5 d after eclosion. For QA induction, 75 mg QA (or 20 mg for all PI experiments) was dissolved in 300 µl water, evenly applied to the surface of 10 ml food in a small vial, and let dry overnight. Females were used throughout the experiments, except for those shown in **Figures 2a**, **4a**,**d**,**e**, **5c**,**f**, **6c** and **Supplementary Figure 6a**,**b**. Transgenic fly lines described in this publication will be available at the Bloomington Stock Center.

Visual system. For the experiments that contain *tubP-QS* in the cross, the collected flies were transferred onto QA food, and remained there for 3 d. They were either placed on the benchtop exposed to 'ambient light' or enclosed in a dark cardboard box. We quantified the fluorescence in the anterior half of the optic lobes, where we drew identical rectangles in the counterstaining channel and then measured fluorescent intensity in the signal channel.

For the FLP-mediated experiments, flies were raised at 18 °C. Young adult flies were exposed to three 10-min heat shocks at 37 °C, with 2-h intervals in between. They were then kept at ~25 °C for 4 d, the first of which always in dark, and the last three of which subject to different visual experiences. The specific visual stimulations were programmed with Psychtoolbox in Matlab (Mathworks) and delivered with a high-speed monitor designed for optomotor response[59]. The moving gratings were full-contrast sine waves with a spatial period of 2.5 cm and a frequency of 20 Hz, reversing direction every 10 s. The full-field flicker consisted of 8-s blocks of 20 Hz, flipping between black and white, interspersed with 2 s of gray.

Olfactory system. For the PN experiments, antennal removal was performed with forceps while the flies were anesthetized with CO_2, and the control flies were exposed to CO_2 for the same duration. TRIC signal was measured 5 d after surgery. For the artificial activation with dTrpA1, experiment and control flies were collected in 0.6-ml Eppendorf tubes. Each tube contained 2–3 flies, 50 µl food at the bottom, and sealed with cotton instead of the plastic cap for ventilation. The cotton was soaked with 100 µl water to prevent dehydration. The heat-shock program was conducted on a thermal cycler (MJ research, #PTC-200), with 3 s at 37 °C and 27 s at 22 °C, repeating for 24 h.

To measure luciferase activity, three-fly groups were ground up in Glo lysis butter (Promega #E2661), and assayed with Steady-Glo (Promega #E2510) system following the manufacturer's protocols. The luminosity was measured in 96-well plates using a VICTOR^2 multilable counter (PerkinElmer #1420-018).

NPF neurons. We collected males 0–2 d old, and then housed them for 4 d either by themselves or with an equal number of virgins with daily replenishment. We quantified fluorescent intensity in the topmost layer in the fan-shaped body that has TRIC signal, and only included the anterior part down to the slice where the layer splits into bilateral lobes. We combined data from two independent experiments by aligning the overall mean.

PI cells. The collected flies we placed on QA food for 1 d, and on the second day they were exposed to different conditions. The 'starve' condition was an empty vial with water-soaked Kimwipe. For each yeast/sucrose feeding experiment, the specified amounts were added to 10 ml water in a small vial, in addition to 0.15 g of agar. They were heated in a microwave oven until boiling, and left at ~25 °C to solidify. For each OA/mianserin experiment, the specified amounts were freshly dissolved in 1.5 ml water, and applied to a Kimwipe in an empty vial. The yeast-OA interaction experiments were water-based, where the dry yeast was boiled with water, and the supernatant after centrifugation was obtained to apply to a Kimwipe.

Computational alanine scanning of MKII. We also explored the potential of *in silico* optimization. To do this, we used the Robetta server to simulate the change of binding energy caused by each alanine mutation in MKII[60]. Although no correlation was found between *in vitro* and *in silico* alanine scan mutagenesis when we considered all variants (data not shown), significant correlation emerged when we excluded variants in which a charged residue was mutated to alanine ($P = 0.0265$; **Supplementary Fig. 7d**). This is consistent with previous knowledge that Robetta performs better with non-charged residues[60], and suggests that future optimization may be aided by a computational exhaustion of the parameter space.

For the simulation in the next section, we estimated the affinity of MKIIK11A, a mutation to a charged residue, as follows. In the S2 cell assay, signal from the MKIIK11A variant belongs to 'Rank 2', so we estimated the change of binding energy caused by K11A, as the mean of the Robetta predictions for the three non-charged residues in the same 'TRIC signal = 2' column (**Supplementary Fig. 7d**). As a result, $K_{CaM/MKIIK11A}/K_{CaM/MKII} = 1.838$.

Simulating TRIC signals. The TRIC signal in **Figure 4b** and **Supplementary Figure 7** was calculated as follows.

Independent variables. $[Ca^{2+}]$: Ca^{2+} concentration (normalized to the dissociation coefficient between Ca^{2+} and CaM). [AD]: the total number of AD::CaM proteins (normalized to the dissociation coefficient between DBD and its target sequence). [DBD]: the total number of peptide::DBD proteins (normalized to the dissociation coefficient between DBD and its target sequence). [CaM]: the total number of endogenous CaM (normalized to the dissociation coefficient between DBD and its target sequence). [peptide]: the total number of endogenous CaM-target peptide (normalized to the dissociation coefficient between DBD and its target sequence).

Parameters. $K_{CaM/peptide}$, $K_{CaM/MKII}$, $K_{CaM/MKIIK11A}$: dissociation coefficients between Ca^{2+}-bound CaM and endogenous target peptides, MKII and MKIIK11A, respectively (normalized to the dissociation coefficient between DBD and its target sequence).

Initialization. [DBD] = 1.5 (for "1 DBD"), [AD] = 1.5 (for "1 AD"), [CaM] = 1.5 (for "1 × competition") and [peptide] = 1.5 (for "1 × competition"). We arbitrarily set $K_{CaM/MKII} = 1$, and the corresponding $K_{CaM/MKIIK11A} = 1.838$ according to the estimation described in computational alanine scanning.

Assumptions. $[Ca^{2+}]$ >> [AD] + [CaM]. Complete cooperativity between the four Ca^{2+}-binding sites on CaM, as illustrated in **Figure 1a**. [DBD] >> its target sequence. $K_{CaM/peptide} = K_{CaM/MKII}$.

Calculations. $[CaM•Ca^{2+}] = ([AD] + [CaM]) \times [Ca^{2+}]\text{^}4 / (1 + [Ca^{2+}]\text{^}4)$, find the solution to $[DBD•CaM•Ca^{2+}]$ following five equations.

$$[DBD]_{free} \times [CaM•Ca^{2+}]_{free} / [DBD•CaM•Ca^{2+}] = K_{CaM/MKII} \text{ (or } K_{CaM/MKIIK11A})$$

$$[DBD]_{free} + [DBD•CaM•Ca^{2+}] = [DBD]$$

$$[peptide]_{free} \times [CaM•Ca^{2+}]_{free} / [peptide•CaM•Ca^{2+}] = K_{CaM/peptide}$$

$$[peptide]_{free} + [peptide•CaM•Ca^{2+}] = [peptide]$$

$$[CaM•Ca^{2+}]_{free} + [DBD•CaM•Ca^{2+}] + [peptide•CaM•Ca2^{+}] = [CaM•Ca^{2+}]$$

then:

$$signal = [DBD•CaM•Ca^{2+}]/(1+[DBD]) \times [AD]/([AD] + [CaM])$$

Immunohistochemistry. Brains were dissected and stained following standard procedures[61]. Primary antibodies: Mouse nc82 (DSHB mAbnc82, 1:30), chicken anti-GFP (Aves Labs GFP-1020, 1:1,000), rabbit anti-dsRed (Clontech 632496, 1:500). Brains from the same condition were processed within the same tube.

© 2015 Nature America, Inc. All rights reserved.

Imaging brains. Images were taken on LSM 510 or 780 confocal microscopes with 20× objectives (Zeiss). For experiments in the same panel, we adjusted the gain so that the sample with the strongest signal barely saturates the dynamic range of the PMT, and imaged all the brains with the same settings and as close as possible time-wise. We did not adjust the offset.

Image analysis. Images were analyzed with Fiji. For fluorescence intensity quantification, the Z stacks of the sum of TRIC signals were generated. We then manually selected the region of interest (see details under the subheadings for each manipulation) to measure the total intensity.

Comparisons were made between data collected either from parallel experiments, with exactly the same master mix of solutions, timeline and imaging conditions, or from different batches of experiments normalized to common controls. For example, data for **Figure 6g** were collected separately, but within each batch there was always one group of *MKIIK11A::GAL4DBDo > mCD8::GFP* exposed to 10% yeast, whose signal intensity served as the common denominator. Each experiment was repeated at least twice, and we only presented qualitatively consistent results. The data passes Jarque-Bera test whenever normality was assumed.

Custom Matlab scripts were used to assist the averaging of medulla images. The confocal stacks were loaded into Matlab. For each sample, we visually selected a slice corresponding to the same anterior-posterior position according to the nc82 counterstain pattern. Matlab then masked the image using a user-defined threshold. We manually selected the block of neuropil corresponding to the medulla, and Matlab traced its outline. We then specified the outer and inner rims of the medulla by clicking on their starting and ending points, and Matlab generated ten equally spaced control points on each rim. These twenty control points were used to register the medulla to a common fan-shaped template. After registration, the sums of all pixel-by-pixel fluorescent intensities within medulla were used for **Figure 2e**. For **Figure 2f**, we pooled data into ten evenly spaced bins along the proximal-distal axis (which do not exactly correspond to the 10 layers), and added the fluorescent intensities within each bin. The total signal intensity in each bin was then normalized to the overall sum.

Statistics. No statistical methods were used to determine sample sizes, but our sample sizes are similar to those generally employed in the field. Individual flies were randomly assigned to treatment groups. Data collection and analysis were not performed blind to the conditions of the experiments.

A **Supplementary Methods Checklist** is available.

51. Tian, L. *et al.* Imaging neural activity in worms, flies and mice with improved GCaMP calcium indicators. *Nat. Methods* **6**, 875–881 (2009).
52. Montigiani, S., Neri, G., Neri, P. & Neri, D. Alanine substitutions in calmodulin-binding peptides result in unexpected affinity enhancement. *J. Mol. Biol.* **258**, 6–13 (1996).
53. Bischof, J., Maeda, R.K., Hediger, M., Karch, F. & Basler, K. An optimized transgenesis system for *Drosophila* using germ-line-specific phiC31 integrases. *Proc. Natl. Acad. Sci. USA* **104**, 3312–3317 (2007).
54. Berdnik, D., Chihara, T., Couto, A. & Luo, L. Wiring stability of the adult *Drosophila* olfactory circuit after lesion. *J. Neurosci.* **26**, 3367–3376 (2006).
55. Sweeney, L.B. *et al.* Temporal target restriction of olfactory receptor neurons by Semaphorin-1a/PlexinA-mediated axon-axon interactions. *Neuron* **53**, 185–200 (2007).
56. Smith, H.K. *et al.* Inducible ternary control of transgene expression and cell ablation in *Drosophila*. *Dev. Genes Evol.* **206**, 14–24 (1996).
57. Lai, S.L., Awasaki, T., Ito, K. & Lee, T. Clonal analysis of *Drosophila* antennal lobe neurons: diverse neuronal architectures in the lateral neuroblast lineage. *Development* **135**, 2883–2893 (2008).
58. Hombría, J.C., Brown, S., Hader, S. & Zeidler, M.P. Characterization of Upd2, a *Drosophila* JAK/STAT pathway ligand. *Dev. Biol.* **288**, 420–433 (2005).
59. Katsov, A.Y. & Clandinin, T.R. Motion processing streams in *Drosophila* are behaviorally specialized. *Neuron* **59**, 322–335 (2008).
60. Kim, D.E., Chivian, D. & Baker, D. Protein structure prediction and analysis using the Robetta server. *Nucleic Acids Res.* **32**, W526–W531 (2004).
61. Wu, J.S. & Luo, L. A protocol for dissecting *Drosophila melanogaster* brains for live imaging or immunostaining. *Nat. Protoc.* **1**, 2110–2115 (2006).

© 2015 Nature America, Inc. All rights reserved.

doi:10.1038/nn.4016